IEEE Access
Multidisciplinary | Rapid Review | Open Access Journal

Received June 12, 2019, accepted June 25, 2019, date of publication June 28, 2019, date of current version July 15, 2019.

Digital Object Identifier 10.1109/ACCESS.2019.2925682

Fabrication, Characterization and Control of Knit-Covered Pneumatic Artificial Muscle

BABAR JAMIL, SEULAH LEE, AND YOUNGJIN CHOI, (Senior Member, IEEE)
Department of Electrical and Electronic Engineering, Hanyang University, Ansan 15588, South Korea

Corresponding author: Youngjin Choi (cyj@hanyang.ac.kr)

This work was supported in part by the Robot Industry Core Technology Development Program funded by the Korean Ministry of Trade, Industry and Energy, under Grant 10080336, and in part by the Convergence Technology Development Program for Bionic Arm through the National Research Foundation of Korea funded by the Ministry of Science, ICT and Future Planning, South Korea, under Grant NRF-2015M3C1B2052811.

ABSTRACT This paper presents the design, fabrication, characterization, and validation of three kinds of knit-covered pneumatic artificial muscle (called k-PAM) actuators, in which three different knits are made by braiding silver-plated (conductive) yarn and non-conductive yarns with different stitch methods. After a successful characterization process, these k-PAM actuators are able to provide feedback information on actuator length corresponding to the applied pressure. A complete fabrication method is proposed to make the actuator work for higher pressures (up to 300 kPa or more). Furthermore, since the force generated by the actuator is decoupled from the external force, ultimately, it can be directly used to measure both the length and the force. This paper contains the detailed characterization processes, the experimental validations of the sensing ability, and the several characteristics of the k-PAM actuators. It is expected that the k-PAM actuator can be used directly for robotic applications in higher pressure conditions, while the semi-permanent conductive knit cover provides the actuator with durability in highly repetitive situations.

INDEX TERMS Conductive knit cover, pneumatic artificial muscle, sensing, control.

I. INTRODUCTION

Artificial muscle is one of the well-established terms in the field of soft robotics and the first attempt to understand this behavior can be found in [1], [2]. This artificial muscle is actuated in such a way that the volume inside actuator changes using pneumatic or fluid pressure. The actuator using the pneumatic pressure is referred to as Pneumatic Artificial Muscle (PAM). These actuators are able to exert hundreds of newtons of force depending on the actuator dimensions and applied pressures. In the traditional approach, however, mechanical joints are usually operated by hard actuation systems with electric current and voltage to be used for higher bandwidths and rapid responses. The recent advent of soft robotics and the interest in making human-robot interaction much safer in the fields of healthcare, rehabilitation, [3]–[6] and their use in robotic devices, which are currently in the testing phases. The PAM actuators provide flexibility in design modification because their fabrication is performed using the elastomer based on mold manufacturing. However, their control performance is not so very good due to the flexibility of PAM itself and the lack of appropriate sensing technology regarding considering length change and output force. In addition, it has been reported in [7], [8] that estimating the actuator length change enables us to estimate the output force.

PAM actuators are mostly fabricated and assembled using physical connections between an elastic body (bladder) and various types of additives such as plastic mesh or fabric to change the properties of these actuators, as well as enhance their performance in terms of hysteresis and maximum output force. The elastic part is hollow inside and known as an elastic bladder, which is fabricated using hyper-elastic materials like elastomer. Additives consist of a semi-inextensible plastic mesh or fabric, which is used on the bladder to cover the entire body of the actuator. Movement at the output end of the actuator is produced through a combination of the aforementioned two types of components. Expansion of the bladder is resisted by a semi-inextensible additive when the PAM makes a contraction in the longitudinal direction. The total contraction quantity is referred to as a stroke of the PAM. The braided PAM is one of the most famous actuators because of its ability to generate large amounts of forces with stable actuation. Different sizes of the braided mesh covers can

The associate editor coordinating the review of this manuscript and approving it for publication was Huanqing Wang.

be selected to vary the total stroke of the actuator, and the thickness of the bladder walls and diameter of the braided mesh can also be varied to tune the relationship between output force and stroke. In recent years, there has been a lot of theoretical progress, such as the development of analytical methods to find the relationship between pressure and force under specific conditions of the length and other parameters [7]–[10].

Many researches have recently demonstrated that the use of strain sensors with PAM actuators could make complex pneumatic control easier. Among these designs and proposals, Park et al. proposed the use of EGaIn (Eutectic Gallium Indium) micro-channels embedded in the elastic outer layer of the actuator body in [11]. This outer layer was thus responsible for sensing the strain or contraction of the actuator body, while Kevlar threads in the inner body of the actuator prevented expansion due to the inside pressure. This idea of using EGaIn-based sensors for PAM actuators has been one of the main recent topics to provide PAM actuators with sensing abilities [12], [13]. While these schemes are promising for practical use, it is uncertain that they can be useful under repetitive operating conditions and high-pressure environments because EGaIn micro-channels are fragile and prone to leak due to large strains in the actuator body. In a similar context, there have been other works that measure the contraction directly from these actuators. Some of these include conductive fiber applications to create variable resistors, and ultimately, to measure the resistance changes due to contractions of these PAM actuators in [14], [15]. These have shown very promising results in handling large forces when compared to braided PAM actuators, however, further works have not been carried out. On the other hand, a scheme to estimate the contractions of a PAM actuator has been suggested in [16].Though there have been many studies and outcomes, many research issues still remain, for instance, to make less bulky and easy to fabricate PAM actuators. In addition, various closed-loop control schemes for PAM actuators such as nonlinear PID control, optimal control, model-based control, and other control strategies for unmodeled systems have been proposed in [17]–[19], [24], [25], for higher control performance.

Motivated by the above concerns and inspired by the proprioceptive sensing ability of human muscles, we design, manufacture, characterize and control artificial pneumatic muscles. Note there have been numerous studies done in regard to these topics. Especially, manufacturing such actuators with stable and long cycle lives is among the difficult issues to be resolved. However, the stability of the conductive knit fabric cover provides a huge advantage when repeated actuation is required. In our experiments, the actuator was verified over several thousands of cycles without any observable physical degradation. The main problems of actuators are related to the design of a highly repeatable conductive cover for these pneumatic muscles, in addition to the stability, design flexibility, and characterization of such actuators, which are addressed in this paper.

Knit-based soft fabrics have been a new trend in the field of smart sensing clothing, including health monitoring and sur-face electromyography (sEMG) signals measurement. These fabric-based sensing devices have shown promise because of their smaller cost, good repeatability, and easy design alterations [20]–[23]. Such knitted fabrics can be used as semi-inextensible covers for the elastic bladders. The conductive fabric is knitted with conductive yarn and stretchable spandex together to make it semi-stretchable. This paper presents PAM actuators with conductive knit covers that can be used in three different configurations. These configurations are called types *A*, *B*, and *C* knit-covered PAM (in short, k-PAM) actuators according to the different type of knit covers considered in this paper. A new fabrication method is introduced to make the actuator strong enough so that it can be operated under high pressure conditions and repetitive environments, as discussed in Section II. The effectiveness of the proposed design and fabrication are verified through several calibration and control experiments. For these purposes, instrumental setups for calibration, modeling, and control verification are illustrated in Sections III and IV. The closed-loop control scheme of the k-PAM actuators using direct sensor feedback is also presented to verify that these covers are useful as real-time sensors in Section V. Finally, discussion of the results is given in VI.

II. FABRICATION OF K-PAMS

The main objective of our study is to fabricate conductive knit covers for the PAM bladder to provide it with the capability for sensor feedback directly from the outer surface of the actuator. Knitting is a sort of fabric making process by interlocking loops of yarns with each other; in particular, the knit (namely, knitted fabric) is more stretchable than the woven fabric thanks to the interlocking space of each loop in every stitch, as illustrated in Fig. 1. To study the sensitivity variations according to knitting structure, two kinds of stitching methods are adopted, as shown in Fig 2. Fig. 2(a) shows the plain stitch using a basic knitting technique. The plain stitch (also called a jersey, flat, or stockinette stitch) is much flatter and lighter than other knitted structures. It is also able to withstand high tensile forces. The manufacturing technique for the plain stitch with conductive yarn will be

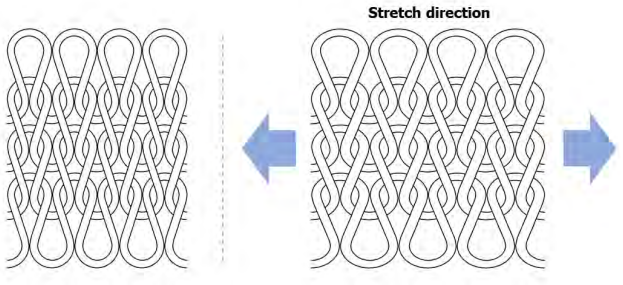

FIGURE 1. Stretchability of the knit by interlocking loops of yarns each other.

TABLE 1. Specifications and materials of knit-based strain sensing covers according to types, where the conductive yarn for all the types is 99% pure silver-plated polyamide yarn with an electric resistance of 3,000Ω/m.

	type A	type B	type C
non-conductive material	spandex	spandex	8 carrier braid used Dyneema spun
stitching method	rib	plain	plain
knitting machine	flat knitting machine	circular knitting machine	hand-held circular knitting device
use for braided mesh	no	yes	no

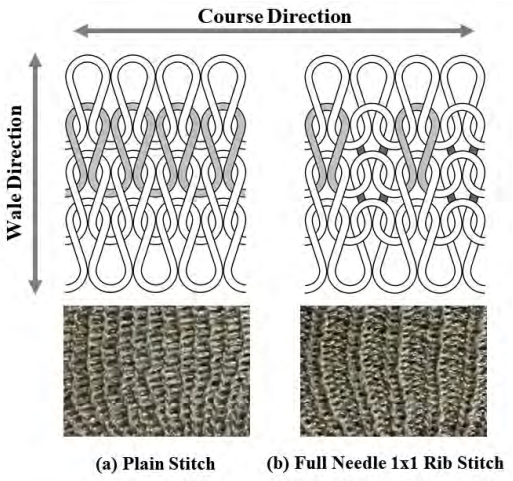

FIGURE 2. Schematics of knits according to different stitching methods, (a) plain stitch, (b) rib stitch, where the dark-colored area implies the silver-plated (conductive) yarn and the white-colored area denotes non-conductive yarn (spandex).

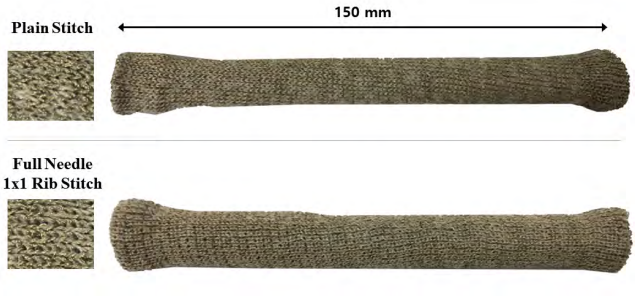

FIGURE 3. Prototypes of knit-based strain sensing covers, where the topmost denotes type *A*, the middle *B*, and the bottom *C*. The knitting patterns are magnified to show how the conductive and non-conductive yarns are mixed. Additionally, the top and middle are manufactured using an industrial knitting machine, while the bottom is made using a hand-held circular knitting device.

explained in subsequent sections. Fig. 2(b) shows the full needle 1×1 ribbing stitch (in short, the rib stitch), which consists of vertical stripes obtained using plain stitches and reverse plain stitches alternately. It is more stretchable in the lateral direction (i.e., the wale direction shown in Fig. 2) than the course direction. Apart from the stitching method, an inextensible yarn is used to make a new type of conductive knit cover. In summary, the properties of three types of conductive covers are investigated, as shown in Fig. 3. These knit covers are different from each other and utilized for k-PAM actuators. For the sake of simplicity, k-PAM with the rib stitch cover is called type *A*, k-PAM with the plain stitch cover and braided mesh is called type *B*, and k-PAM with the plain stitch cover and a mixture of inextensible fiber and conductive yarn is called type *C*. Their basic specifications and materials are listed in Table 1. Although the conventional method is adopted to make actuator bladders, the entire processes for fabricating types *A*, *B* and *C* k-PAM actuators are explained in the next sections.

A. TYPE A K-PAM ACTUATOR

Type *A* k-PAM actuators are made using the rib stitch for standalone actuation, which refers to the fact that additional inextensible layers are not required other than the knit cover on the bladder, where the cylindrical knit cover is made by braiding the spandex and the silver-plated yarn using a flat knitting machine originally intended for industrial purposes. The whole fabrication procedure of the type *A* k-PAM actuator is illustrated in Fig. 4, beginning with fabrication of the PAM bladder. For this, Dragon Skin 30 A/B were mixed at a 1:1 ratio and filled into the mold for the actuator bladder. The molded silicone was then degassed for 10 minutes and left in an oven at $150°F$. Two major specifications of the fabricated soft body bladder are its diameter and length, which determine the overall behavior of the actuator. The bladder has a total length of $150mm$ and diameter of about $13mm$. Then, the cylindrical knit cover is assembled over the bladder. The next step is to block one side of the bladder while maintaining the effective length of $110mm$ and a hose is then attached at the opposite side of the bladder to supply air pressure. Copper strips are attached and glued on both sides over the knit cover at the effective length, and then the electric wires are soldered over these strips. The wires are terminals to measure the electric resistance change according to the volumetric change of the bladder. One-touch fitting is attached to one side of the actuator, which makes it easy to connect and remove the pneumatic tubing to the actuator. Thus, the cover is easily replaceable in case of device failure. The fabrication process is finalized by fixing clamp locks on the copper strips. The connecting hose was sealed at one end to protect the silicone area. A prototype of the type *A* k-PAM actuator is shown in Fig. 5.

B. TYPE B K-PAM ACTUATOR

Fabrication of the type *B* k-PAM actuator is very similar to that of type *A* k-PAM, except for the differences listed in Table 1. A plain stitch cover made using a circular knitting

FIGURE 4. Fabrication and assembling processes of type *A* k-PAM actuator.

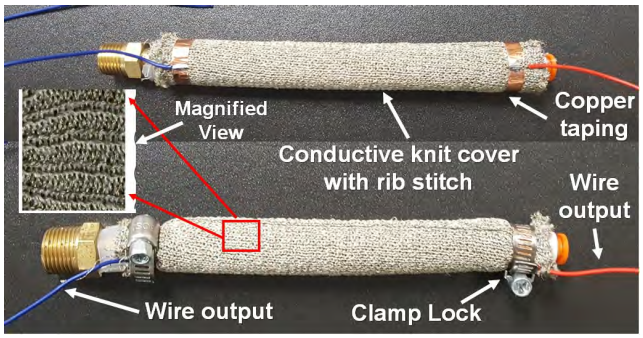

FIGURE 5. Type *A* k-PAM actuator prototype.

machine for industrial purpose is used instead of the rib stitch for type *A*. Since the plain stitch cover is highly flexible in all directions, it allows for easy volumetric changes of the bladder. Thus, the braided mesh is additionally covered on the plain stitch cover, as shown in Fig. 6 to prevent being blown up. For comparison of types *A* and *B*, their effective lengths and diameters were maintained similar to each other.

C. TYPE C K-PAM ACTUATOR

The type *C* k-PAM actuator is designed by adopting the advantages of types *A* and *B* k-PAM actuators, in the sense that the plain stitch cover is used, but the braided mesh is not required due to an inextensible fiber (8 carrier braid used Dyneema spun) being used instead of spandex for types *A* and *B*, as listed in Table 1. Additionally, note that the conductive yarn for all types is 99% pure silver-plated polyamide yarn with an electric resistance of $3{,}000\Omega/m$, but can be plated with different metals such as copper. For our specific experimental studies, a hand-held circular knitting device with 9 needles (shown in Fig. 7) is chosen to fit the diameter of the PAM actuator ($15mm$). The conductive and non-conductive yarns are knitted together by interlocking loops and running the device until the target length is

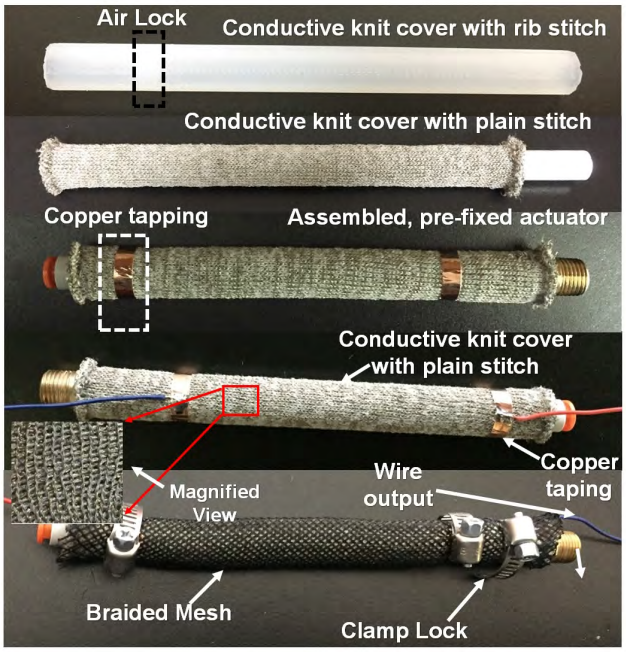

FIGURE 6. Fabrication and assembling processes of the type *B* k-PAM actuator and its prototype.

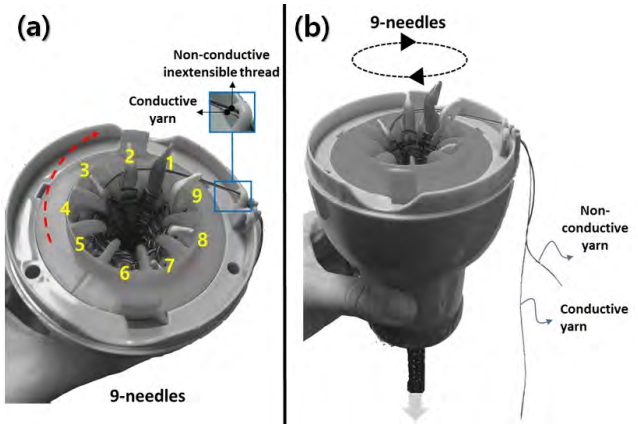

FIGURE 7. Hand-held circular knitting device with 9 needles; (a) two kinds of yarns are loaded into the needles, including conductive yarn and non-conductive inextensible yarn; (b) the circular knitting process.

achieved, as shown in Fig. 7(b). A prototype of the type *C* k-PAM actuator is shown in Fig. 8.

III. EXPERIMENTAL SETUP FOR K-PAM ACTUATORS

The force equation for a cylindrical PAM actuator is presented in the following form:

$$F = -P\frac{dV(L_e)}{dL_e} \tag{1}$$

where P is the pressure inside the bladder with diameter D, L_e denotes the effective length of bladder, and V is the volume of bladder as a function of L_e:

$$V = \frac{\pi}{4}D^2L_e \tag{2}$$

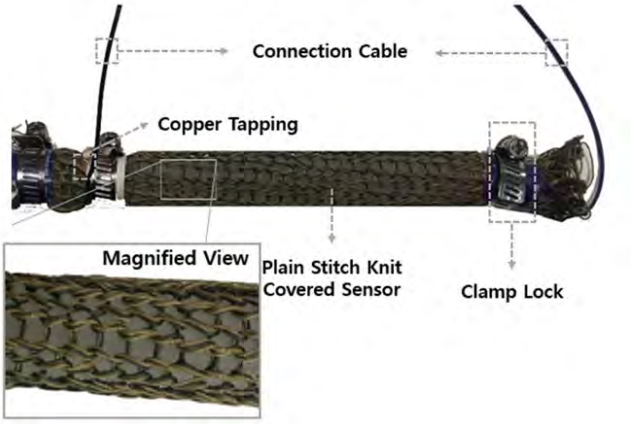

FIGURE 8. Type *C* k-PAM actuator prototype.

in which, since dL_e is related to the stroke variable, $dV(L_e)$ is directly dependent on the stroke variable. Thus, it is referred to as volumetric change due to stroke variation. In our studies, not only the contracting strain is measured, but also the extending strain. For this purpose, an experimental setup is developed for calibration and signal acquisition, as explained in later sections.

A. EXPERIMENTAL SETUP TO MEASURE THE RESPONSE OF K-PAM WHEN STRAIN IS EXTERNALLY PROVIDED

To provide the strain with k-PAM externally, a linear actuator (Firgelli P16-100-22-12-P) and its corresponding control components such as motor driver and microprocessor were used as shown in Fig. 9.The linear actuator was controlled via the position control mode using potentiometer feedback. Target strains ranged from 0 to 10mm. The electric resistance variations according to k-PAM elongation and contraction were first amplified and measured using the Wheatstone bridge circuit since the electric resistance of the conductive knit was very small. All data were sampled and processed using the data acquisition board (NI DAQ-6216), and the same device was used as a general analog output for controlling the pneumatic pressure regulators. In detail, the length variation *vs* resistance change were recorded in real-time and

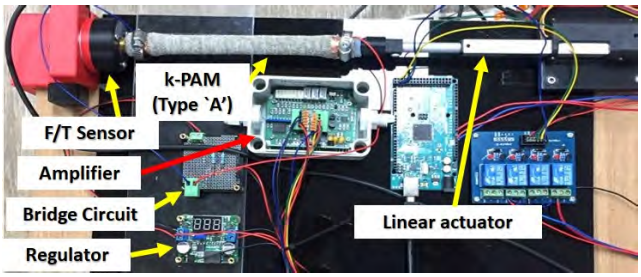

FIGURE 9. Experimental setup to measure the strain offered by the linear actuator located outside.

the data were then plotted to analyze the response of the k-PAM actuator under externally provided strain.

B. CALIBRATION SYSTEM

Calibration of the system (i.e., a contraction analysis apparatus) was used to determine the characteristics for conductive knit behavior while the k-PAM actuator is supplied with pressure. The whole calibration system is divided into three parts: a fixed frame for holding the input side of the k-PAM actuator, a moving frame (i.e., a partially fixed frame) to detect contraction of the k-PAM actuator under loaded and unloaded conditions, and signal processing circuitry including linear sensors. A linear pneumatic pressure regulator ($0 \sim 5V$ control input SMC Pneumatic Regulator, ITV1030) is used to provide a controlled pneumatic source through the tubing connected to the k-PAM actuator. This regulator is controlled using an analog voltage ($0 \sim 5V$) from the Data Acquisition board (NI DAQ-6216). The fixed frame is used as a base and the other side of the k-PAM actuator is connected to the freely moving frame composed of different sensing and loading systems.

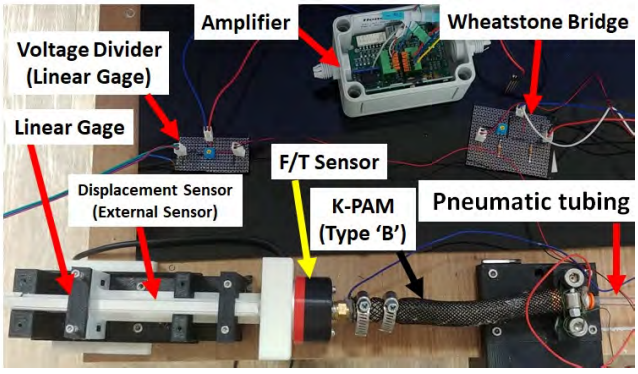

FIGURE 10. Calibration system for the k-PAM actuators.

Fig. 10 shows the side-view and top-view of the entire calibration system, respectively. The sensing system involves a linear position and force sensors, which are attached to the moving end, to read its current position and force signals. This sensing system is fixed in front of a moving frame that provides force feedback when the k-PAM actuator is in the active state. The moving frame has a linear guide to measure relative motion with respect to the fixed frame. Additionally, the moving frame has interfacing points for 3 spring loads at one end to study the characteristics of the k-PAM actuator. The spring loads are used to calibrate and determine the relationship between the force produced by the k-PAM actuator *vs* the known external loads. This calibration system provides information on three important variables, the pressure supplied by linear regulator, the force applied to the moving end, and the length of the k-PAM actuator. Under these conditions, the pressures are varied in the range of $0 \sim P_{max}$ where P_{max} is the pressure such that maximum stroke is achieved (this may vary depending on the loads and

other conditions). In our experiments, P_{max} was always lower than 5 *bar* (equivalent to 500 kN/m^2).

C. SIGNAL ACQUISITION SYSTEM

For linear displacement sensing, a potentiometer and voltage divider circuit were used with the voltage source as, shown in Fig. 11(a), where V_s denotes the constant voltage supply as $5V$, R_l is the current resistance of the potentiometer composed of variable resistors, and R_d is a constant reference resistance in the voltage divider circuit. The voltage value of the reference resistor R_d is read by the data acquisition board for sampling and amplification. After appropriate signal conditioning, an accurate linear displacement x_d is calculated by reading the voltage variation ΔV_{R_d} across the reference resistor R_d as follows:

$$x_d = 100 \cdot (V_{R_{d,i}} - V_{R_{d,c}}) \quad [mm], \tag{3}$$

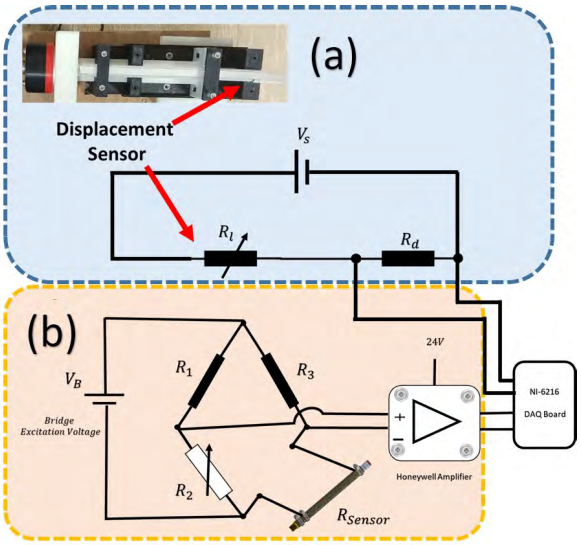

FIGURE 11. Signal acquisition systems including linear displacement and conductive knit cover sensors, with a (a) signal acquisition circuit for the linear displacement sensor, and (b) signal acquisition circuit for the conductive knit cover, including a Wheatstone bridge and analog amplifier, where R_2 is a variable resistor for tuning the bridge circuit.

where $V_{R_{d,i}}$ indicates the initial voltage across R_d when no contraction is applied, and $V_{R_{d,c}}$ denotes the current value of voltage drop across R_d.

Signal acquisition from the proposed conductive knit cover is important because precise data collection is required to construct the mathematical model of the k-PAM actuator. For this, a Wheatstone bridge circuit was chosen for measurement of the electric resistance variations according to volumetric change of the conductive knit cover. The resolution of the ADC (analog-to-digital conversion) for the bridge circuit was chosen to measure four decimal points of variation in the resistance. Fig. 11(b) shows the basic circuit and block diagram for signal acquisition of the conductive knit cover. The entire procedure is as follows:

- In the Wheatstone bridge circuit, two constant resistors R_1 and R_3 were selected with the same value of 100Ω, while R_2 was an adjustable (or variable) resistor with the range of $0 \sim 100\Omega$ to match the resistance of conductive knit cover.
- An LCR meter (LCD-6020) was used to measure the resistance of the conductive knit cover, and then R_2 was accurately tuned to match the resistance of the knit denoted R_{sensor}. The resistance of the knit cover measured using the LCR meter was set to an initial resistance, denoted R_{in}.
- An amplifier with a maximal output voltage of $\pm 10V$ was used to amplify the analog signal (Honeywell vehicle amplifier).
- A data acquisition board (NI-6216) was used for data sampling during actuation.
- The equation for measuring the resistance of the conductive knit cover was derived as follows:

$$R_{sensor} = \frac{(R_2R_3 + R_3(R_1 + R_2)(V_e/V_b))}{R_1 - (R_1 + R_2)(V_e/V_b)}, \tag{4}$$

where V_b is the bridge excitation voltage and V_e denotes the voltage difference between V_2 and V_1. Note that the signals were acquired at the sampling frequency of $3kHz$.

IV. CHARACTERISTICS OF THE K-PAM ACTUATORS

Utilizing the experimental setups suggested in the previous section, several experiments are conducted to determine the characteristics of the k-PAM actuators according to type. The important properties of the k-PAM actuator should be determined, such as its external strain-to-resistance, contraction-to-resistance according to the load conditions, time decay, repeatability, and hysteresis curves. Each of these relative properties is explained and presented for all k-PAM actuators. To begin with, the characteristics of the type *A* k-PAM actuator are examined in terms of the elongation (*i.e.,* external strain) and contraction. For clarity, the relative resistance variation R_{change} is expressed using the following relation:

$$R_{change} = \frac{R_{in} - R_{sensor}}{R_{in}}, \tag{5}$$

where R_{in} and R_{sensor} imply the initial resistance before actuation and the sensing resistance under actuation of the conductive knit cover, respectively.

A. CHARACTERISTICS OF THE TYPE A K-PAM ACTUATOR

1) UNDER THE CONDITIONS OF EXTERNAL STRAINS

When the strain was externally provided, the resistance variations of the type *A* k-PAM actuator were measured using the experimental setup suggested in Fig. 9 and calculated using Eq. (5). Fig. 12 shows the experimental results according to the external strains range of $0 \sim 10mm$ applied to the body of the type *A* k-PAM actuator. In the Fig. 12, the characteristic curve shows an approximately linear behavior. In the figure, note that a negative value implies the resistance increased for the conductive knit cover attached to the type *A* k-PAM actuator.

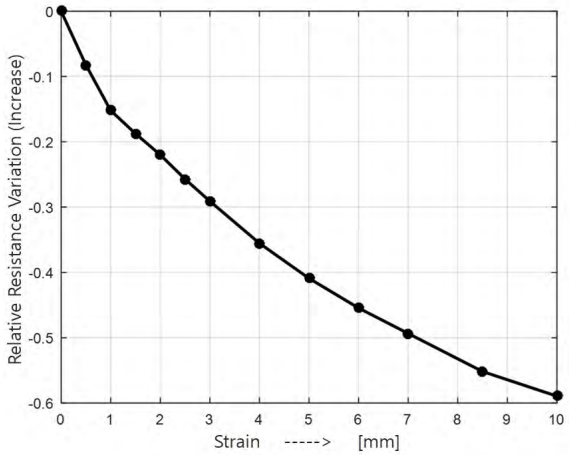

FIGURE 12. Characteristic curve of the type *A* k-PAM actuator between the externally applied strain and the relative resistance variation R_{change}.

2) UNDER THE CONDITIONS OF EXTERNAL LOADS

The characteristics of the type *A* k-PAM actuator under several load conditions were examined using the calibration system suggested in Fig. 10. For external load variations, mechanical springs were attached between the moving and fixed frames when the pneumatic pressure was applied inside the type *A* k-PAM actuator. Note that the external loads were adjusted by changing the number of springs. Fig. 13 shows the relative resistance variation R_{change} according to contraction length. Additionally, we can say that the contraction lengths were approximately proportional to the relative resistance variations R_{change} under constant load conditions.

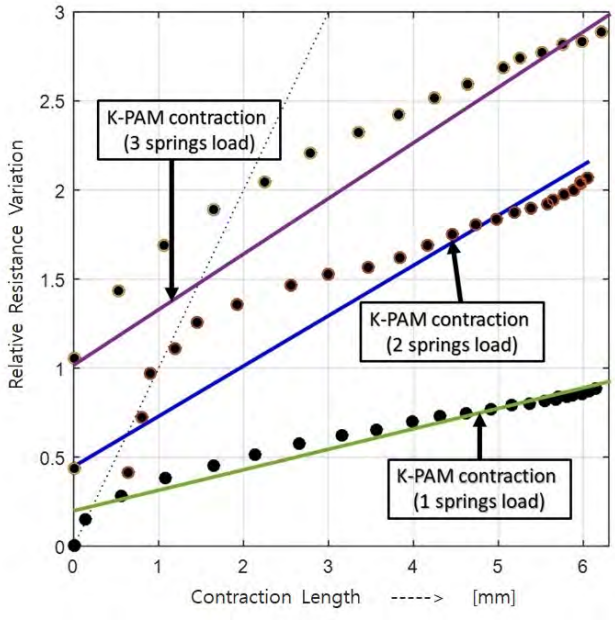

FIGURE 13. Characteristic curves of the type *A* k-PAM actuator between the contraction and the relative resistance variation R_{change} under constant load conditions.

B. CHARACTERISTICS OF THE TYPE B K-PAM ACTUATOR

The characteristics of the type *B* k-PAM actuator are presented in this section. Note that the type *B* actuator was additionally covered with a braided mesh on the conductive knit cover to prevent the bladder from over expansion and material damage. Additionally, the conductive knit cover for type *B* was made via plain stitching to measure the volumetric change of the bladder. The calibration system of Fig. 10 was used to reveal the resistance changes of the conductive knit. For the experiments, four variables (*i.e.,* the resistance of conductive knit, the pneumatic pressure applied to the type *B* k-PAM actuator, the contraction length and the force) are measured using the corresponding sensors. During the measurements, friction existing in the calibration system was ignored, and the pneumatic pressure was supplied with the range of $0 \sim 3.9\ bar$ (equivalent to $0 \sim 390\ kN/m^2$).

1) RELATIONSHIP B/W CONTRACTION AND RELATIVE RESISTANCE

The type *B* k-PAM actuator was tested under four different load conditions as follows:

- without any external load (no spring)
- with low external load (1 spring)
- with medium external load (2 springs)
- with high external load (3 springs)

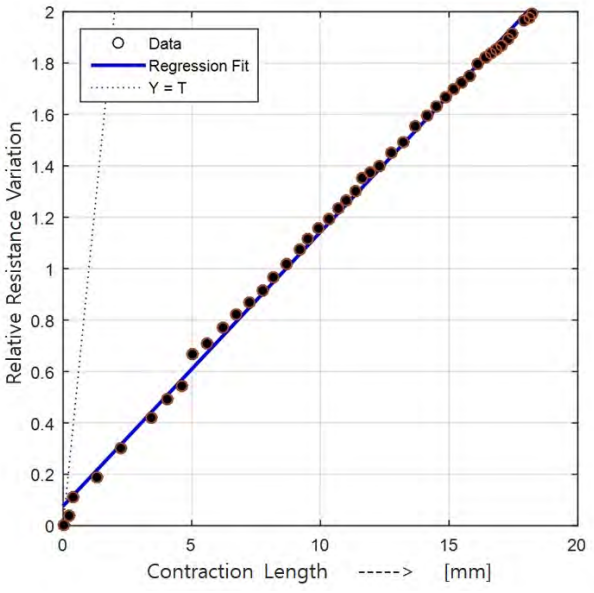

FIGURE 14. Relationship between the contraction and relative resistance variation R_{change} under no load condition, where the type *B* k-PAM actuator was used with the supplied pneumatic pressure of $0 \sim 390\ kN/m^2$.

Fig. 14 shows the relative resistance variation R_{change} of the conductive knit according to the increase in contraction length when an external load was not applied. In the figure, the maximum contraction of the type *B* k-PAM actuator was observed as 18.5 *mm* while the relative resistance variation

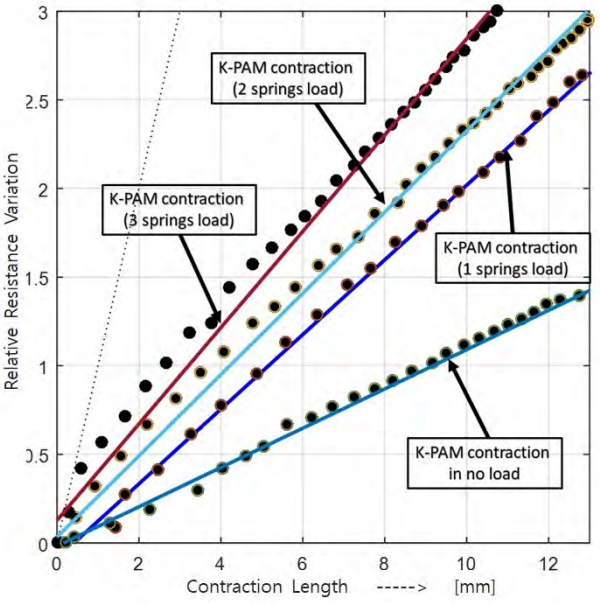

FIGURE 15. Comparisons of the relationships between the contraction and relative resistance variation R_{change} under various external load conditions, where the type *B* k-PAM actuator was used with the supplied pneumatic pressure of $0 \sim 390\ kN/m^2$.

was measured to be around 200% relative to the initial resistance of $R_{in} = 1.4\Omega$.

For the next step, mechanical springs are additionally loaded between the moving and fixed frames, as shown in Fig. 10. All the experiments were repeated with independent observations, and the resultant plots for the comparisons are shown in Fig. 15 as the characteristic curves between the contraction length and relative resistance variation according to the increased external loads. From Fig. 15, we see know that the conductive knit cover of type *B* does not lose linearity in its behavior despite the external load changes. This result could be helpful for calibrating the actuator model. Table 2 summarizes four sets of data for the external loads, including the slopes of linear regressions, maximum contractions, and maximum relative resistance variations.

TABLE 2. Comparisons of slopes for linear regression under the four load conditions.

loaded springs	slope of linear regression	maximum contraction, mm	relative resistance change R_{change}
0	0.111	18.50	2.0
1	0.211	16.30	2.9
2	0.229	12.94	2.9
3	0.272	11.27	2.9

2) RELATIONSHIP BETWEEN PRESSURE AND FORCE/CONTRACTION

The output forces of the type *B* k-PAM actuator according to the supplied pneumatic pressures are plotted in Fig. 16 under three external load conditions. Clear differences in the output force according to the different loads are observed

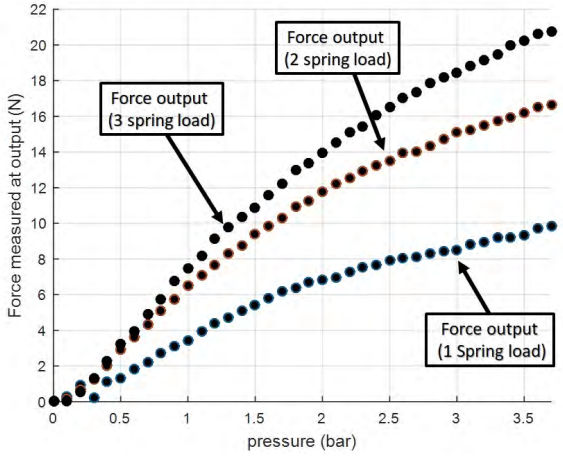

FIGURE 16. Comparisons of the relationships b/w output forces of the type *B* k-PAM actuator and the supplied pneumatic pressures under three external load conditions.

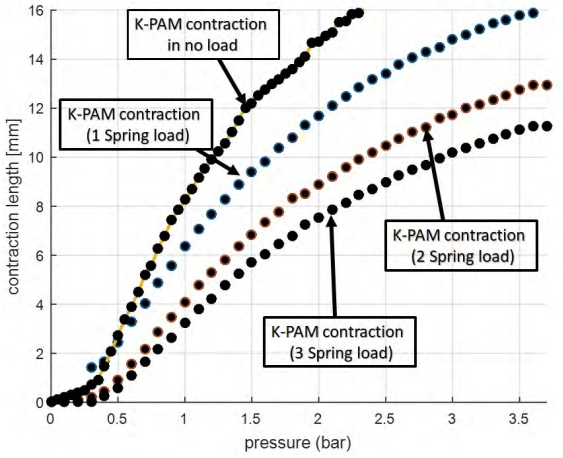

FIGURE 17. Comparisons of the relationships between the contractions of the type *B* k-PAM actuator and the supplied pneumatic pressures under four load conditions.

in Fig. 16. In a similar way, the contractions according to the supplied pneumatic pressures are given in Fig. 17 under four different load conditions. Observe that the contraction is inversely related to the external loads, as indicated in Fig. 17.

3) RISE TIME AND ERROR OF THE TYPE *B* KNIT COVER

The type *B* k-PAM actuator was tested to confirm the rise time and error of the knit cover sensor. Both values are important for closed loop compensation for the actuator output behavior, including force and contraction. Note that the environmental temperature and friction due to volumetric change of the k-PAM can affect the control performance. A step-wise pressure input was applied to the k-PAM actuator and its time responses relative to both the contraction and proposed knit cover sensor output were recorded, as shown in Fig. 18. Here $3bar$ pressure was applied step-wise under the 1 spring load condition and was released after 44 seconds. The knit

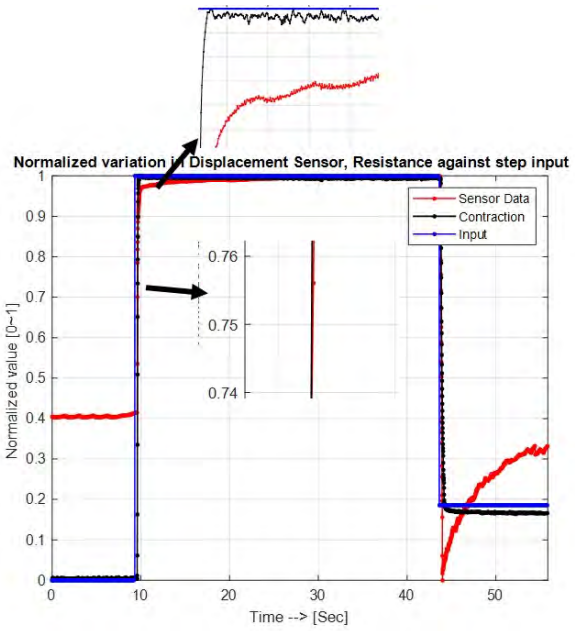

FIGURE 18. Time responses relative to both the contraction and the knit cover sensor output when a step-wise pressure input of 3*bar* was applied to the type B k-PAM actuator under the 1 spring load condition, which was released after 44 seconds.

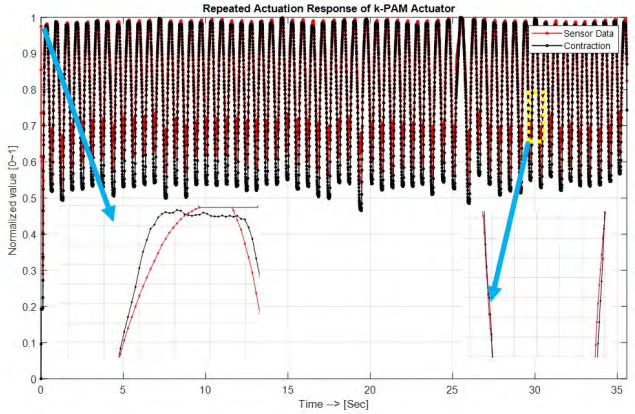

FIGURE 19. Repetitive performance of the type *B* k-PAM knit cover sensor when triangular pressure inputs were repeatedly applied with constant frequency, where the black lines denote the contraction measured by the potentiometer installed in the calibration system and the red lines represent the actual response of the knit cover sensor embedded in the k-PAM.

cover sensor output followed the contraction as measured by potentiometer, with a small rise time less than 10*ms* while reaching over 95% of the final value. This is a very promising result because the knit cover signal reaches its final value after a short time with a small error of less than 5%.

4) REPEATABILITY

This section presents repetitive performance of the type *B* k-PAM knit cover sensor while triangular pressure inputs were repeatedly applied with constant frequency. The actuations were conducted for more than 60 seconds. The contraction measured by the potentiometer and the sensing output of the knit cover are shown in Fig. 19. Thanks to the properties of the fabric, the cover shows good repeatability performance.

5) HYSTERESIS

Hysteresis is an important phenomena in elastomer-based actuation, which is observed in the relationships between force and pressure, force and contraction, and contraction and pressure. The type *B* k-PAM actuator also has a weak hysteresis property between the contraction and sensing output of the knit cover. The experimental results after successive contraction and release phases are shown in Fig. 20. As seen in Fig. 20, the type *B* k-PAM does not show a severe hysteric behavior, but has an approximately linear property during the contraction and release phases.

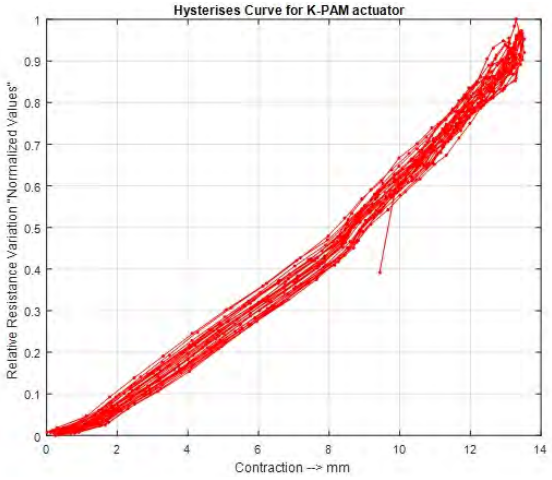

FIGURE 20. Hysteresis behavior of the type *B* k-PAM actuator when successive contraction and release phases were conducted.

C. CHARACTERISTICS OF THE TYPE C K-PAM ACTUATOR

The type *C* k-PAM actuator utilizes the knit cover made using the plain stitching method and a hand-held circular knitting device, without any braided mesh. The characteristics of the type *C* k-PAM actuator under several different load conditions were examined using the calibration system suggested in the Fig. 10, to study the effect of load variations to its response changes. As suggested in the previous sections, the external loads are adjusted by changing the number of springs. Fig. 21 shows the relationship between the contraction and relative resistance variation (R_{change}) in order, to determine the characteristics of the type *C* k-PAM actuator. In the figure, regression fits are also shown for the data, which can be described via nonlinear fitting models. The total contraction was limited to 9 *mm*, but the maximum contraction can be improved further by changing the assembly and fabrication method.

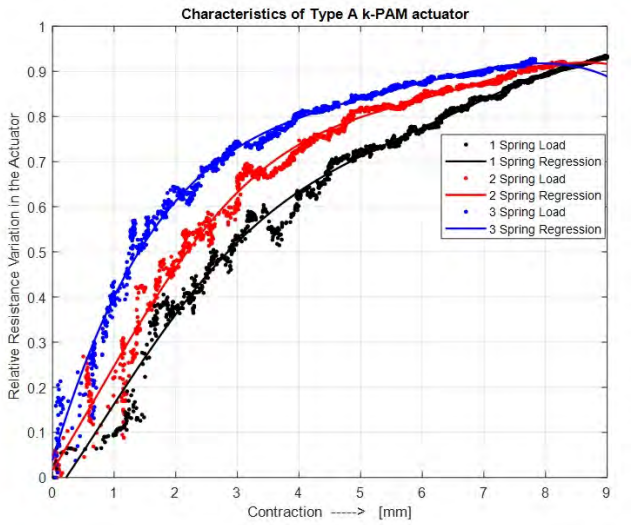

FIGURE 21. Characteristic curves for the type *C* k-PAM actuator between the contraction and the relative resistance variation R_{change} under loaded conditions, where a pneumatic pressure of $0 \sim 350\ kN/m^2$ was supplied.

1) RISE TIME AND ERROR OF THE TYPE *C* KNIT COVER

The knit cover of the type *C* k-PAM actuator is compared with the contraction measured by the potentiometer to confirm the rise time and final error. A step-wise pneumatic pressure input was applied to the type *C* actuator, and its time responses relative to the contraction and knit cover sensor output were recorded, as shown in Fig. 22. Typically, the step response indicates the latency of the knit cover sensor itself as well as its stability against abrupt pressure changes. We experimentally verified that the rise time of the knit cover was less than 10*ms*, with an ignorable error superior to that of the type *B* k-PAM actuator.

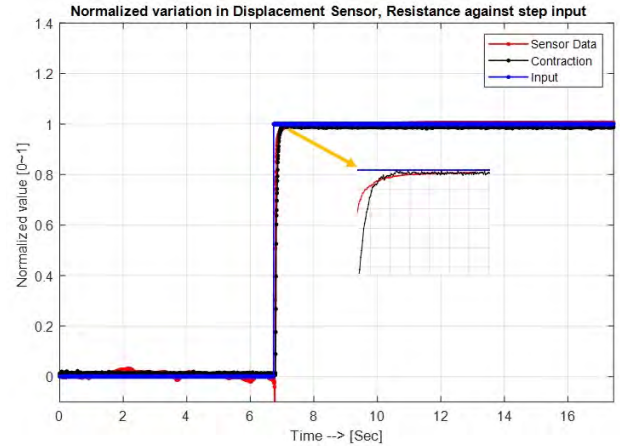

FIGURE 22. Time responses relative to both the contraction and knit cover sensor output when a step-wise pressure input was applied to the type C k-PAM actuator, where the data were normalized.

2) REPEATABILITY

The repetitive performance of the type *C* k-PAM actuator was analyzed through repeated actuations for 60 seconds, similar to the case for the type *B* k-PAM actuator. Triangular pressure inputs were applied to the actuator, and then the contraction and knit sensing output were plotted, as shown in Fig. 23. The sensing output of the knit cover embedded inside the k-PAM closely follows the contraction measured by the potentiometer installed in the calibration system. Thus, we conclude that it shows good repetitive sensing performance.

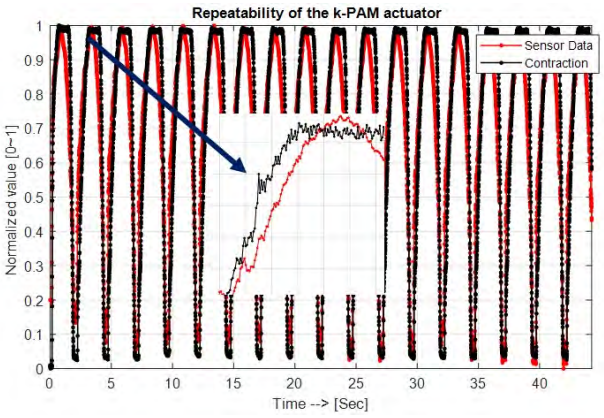

FIGURE 23. Repetitive performance of the type *C* k-PAM knit cover senor with triangular pressure inputs repeatedly applied with constant frequency, where the black lines denote the contraction measured by the potentiometer installed in the calibration system and the red lines represent the actual response of the knit cover sensor embedded in the k-PAM.

3) HYSTERESIS

The type *C* k-PAM actuator showed much clearer hysteresis phenomenon than the type *B* actuator, as suggested in the previous section. For this purpose, repetitive contractions and release actuations with 1 spring load were applied to the type *C* actuator, and the knit sensor outputs according to the contraction lengths were recorded as shown in Fig. 24.

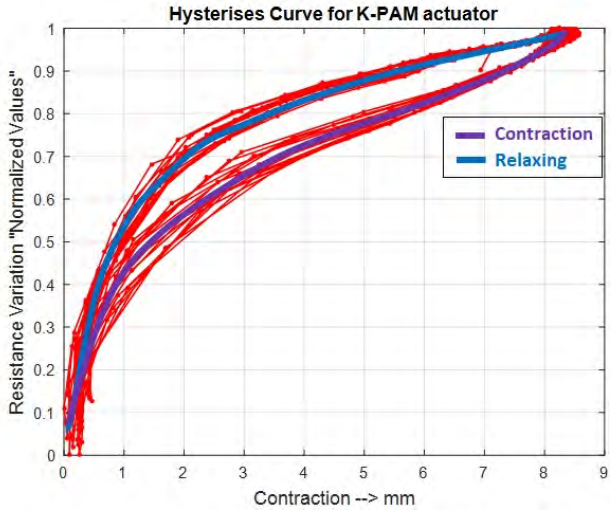

FIGURE 24. Hysteresis behavior of the type *C* k-PAM actuator when successive contraction and release phases were conducted; note that the type *C* actuator has a much clearer hysteresis effect than that of type *B*.

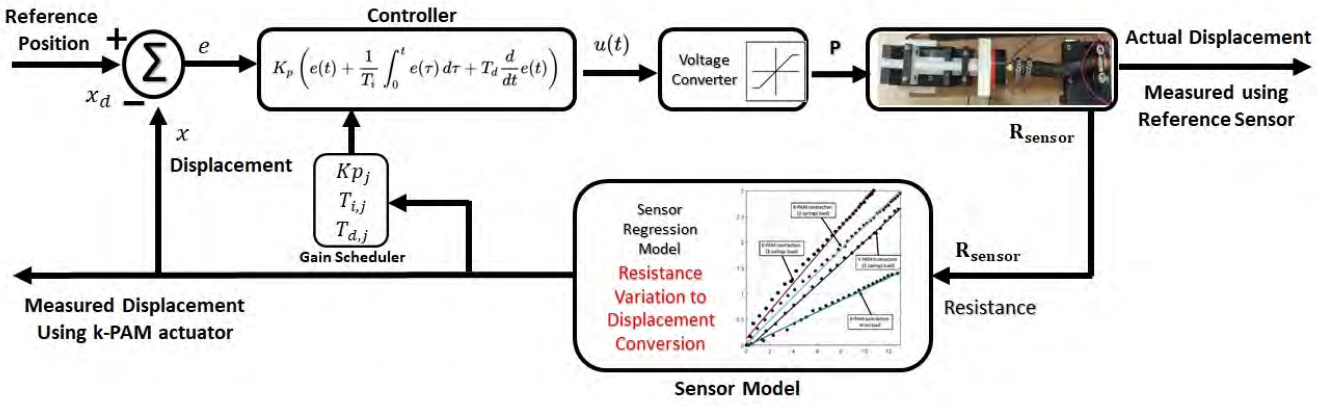

FIGURE 25. Closed-loop position control scheme including gain scheduled PID for the k-PAM actuator, where R_{sensor} is the resistance value measured from the knit cover sensor, x is an actual displacement calculated using sensor model and Eq. (5), and the gains are scheduled according to actual displacements of the k-PAM actuator as suggested in Table 3.

It is important to model and compensate for this nonlinear behavior to achieve good control performance.

V. CLOSED-LOOP CONTROL SCHEME

For practical use, the closed-loop control scheme of the k-PAM actuators is designed to achieve higher performance, as shown in Fig. 25. The type B k-PAM actuator is chosen because it showed superior linearity to the other types. Future studies are expected to utilize the type A and C actuators for different applications. Gain scheduled PID control was adopted to enable easy phase transitions form the input pressure to the contractions, as suggested in Fig. 17. The contractions relative resistance variation of the knit cover sensing output are shown in Fig. 15. The nonlinearity in Fig. 17 requires different gain parameters to achieve higher control performance. In our case, the control gains are divided into three regions and scheduled according to the contraction regions. The gain scheduled PID control was implemented via the switching-based form shown in Fig. 25.

For clarity, the error is denoted by e, the desired (reference) position is represented as x_d and the actual displacement (contraction length) is expressed by x in the Fig. 25. Further, $u(t)$ represented the control input applied to the pneumatic pressure regulator, and is bounded between 0 and $5V$. The sensing output of the knit cover is measured as the resistance R_{sensor} and is converted to the relative resistance variation R_{change} using Eq. (5). Next R_{change} is converted to the actual displacement using linear regression fits. These conversions are dependent on the load conditions applied to the actuator in terms of the slope of linear regression. This actual displacement is fed back into the controller while choosing the appropriate gain parameters according to the contraction regions. In the gain scheduled PID controller shown in Fig. 25, $K_{p,j}$ denotes a proportional gain, $T_{i,j}$ is the integration time, and $T_{d,j}$ is the time derivative for three contraction regions for $j = 1, 2, 3$. The scheduled gain parameters are listed in Table 3 according to the contraction regions.

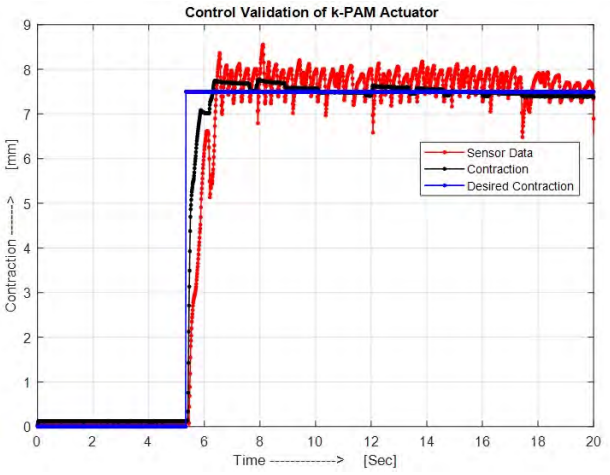

FIGURE 26. Set-point regulation control performance when the proposed closed-loop control scheme is utilized, where the desired contraction is indicated with blue lines and is 7.5*mm* as a step-wise target, the black lines represent the contraction measured by potentiometer installed outside (it is not used in the closed-loop control scheme), and the red lines show the actual displacement calculated using the knit cover sensing output.

Set-point regulation control performance is verified using the calibration system. The experimental results in Fig. 26 indicate that the actual displacement arrives at the set-point (7.5 *mm* of step-wise target) to be regulated. However, observe that the fluctuation of the actual displacement in Fig. 26 interferes with improvement of the position control accuracy. Since the conductive yarn inside the knit cover acts like an electric inductor, it is heavily affected by high frequency noises. The effects of high-frequency noises and resistance fluctuations due to the fabric properties should be suppressed for better regulation control performance. For this, a Butterworth noise filter (low-pass filter) is first applied to the output signal of the knit cover sensor. This Butterworth filter was designed to be fifth-order with a high cutoff of $60Hz$, and low cutoff of $90Hz$, which are much lower than the

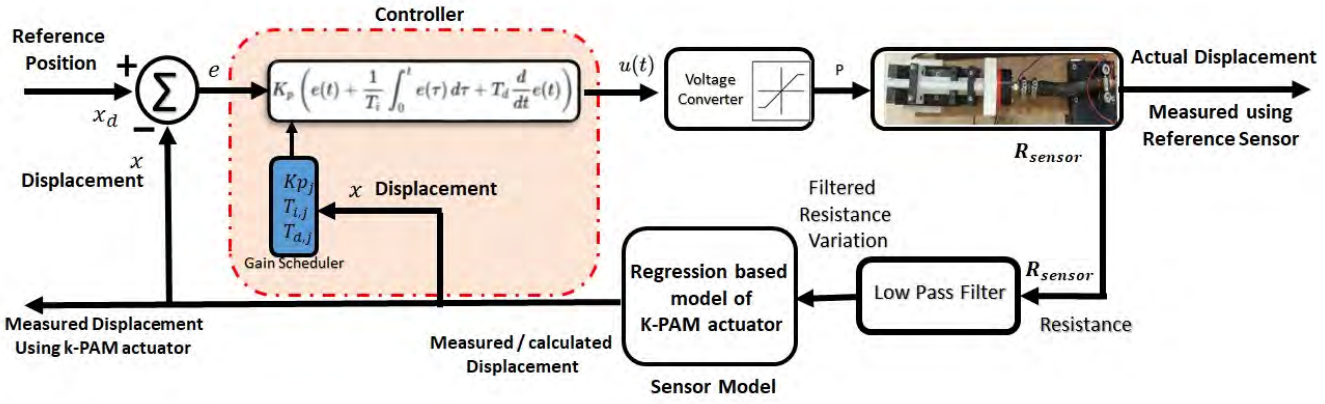

FIGURE 27. Updated closed-loop position control scheme to suppress the effects of high-frequency noises and resistance fluctuations due to the fabric properties.

TABLE 3. Gain scheduled PID control parameters, where K_p, T_i, and T_d denote the proportional gain, integration time, and time derivative, respectively.

j	Contraction Region [mm]	K_p	T_i [s]	T_d [s]
1	[0 ∼ 4.5]	0.24	0.0025	0.00012
2	[4.5 ∼ 10]	0.28	0.003	0.00015
3	[10 ∼ 15]	0.31	0.0028	0.0001

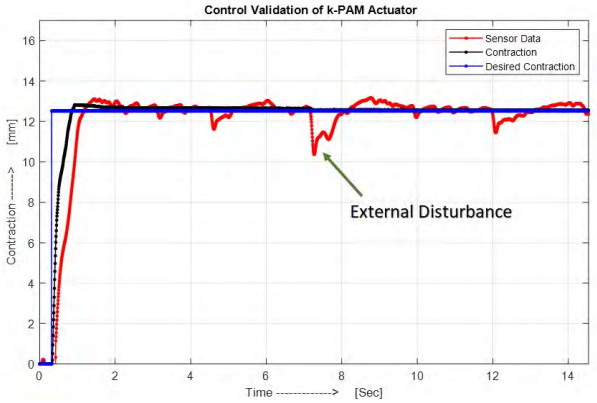

FIGURE 28. Set-point regulation control performance when the updated closed-loop control scheme suggested in Fig. 27 is utilized, where the desired contraction represented by the blue line as 12.52*mm* step-wise target.

control frequency. Second, the averaging filter over 10 samples is applied to the noise filtered signals. The averaged signal is then used to calculate the actual displacement of the actuator. If the aforementioned procedures are added into the control scheme shown in Fig. 25, the updated control scheme can be obtained as illustrated in Fig. 27.

Furthermore, the proportional gain K_p is reduced to 80% of the scheduled value after entering the small error boundary, ultimately making the controller less sensitive to small noises due to fabric resistance fluctuations. After applying the above solutions, we obtained less sensitive experimental results as shown in Fig. 28. Note however that these results were still affected by the resistance change due to the fabric properties. It is expected that the control performance will improve if a higher-order Butterworth filter and different weighted averaging filter techniques are applied.

VI. DISCUSSION

Three types of knit-covered PAM (k-PAM) actuators were presented in this paper based on independent knit designs, fabrication, and assembling methods. In addition, a calibration system was proposed to study the behaviors of all actuator types. Experimental results showed that the k-PAM actuators depended on three main characteristic curves: the relative resistance *vs* contraction, the output force *vs* supplied pressure, and the contraction *vs* supplied pressure, and the contraction *vs* supplied pressure, under various external load conditions. The results showed satisfactory behavior, indicating that these k-PAM actuators could be used in different robotic applications. Improved quality and sensitivity of these conductive knit covers might result in better data acquisition for modeling, and different filtering strategies might be needed to effectively used these effectively. The regression fits showed that these k-PAM actuators could be calibrated to different loads. Further, these conductive knits worked well for both contraction and strain sensing. In fact, the type *A* k-PAM actuator showed its performance limitation in terms of maximal contraction due to the absence of a braided mesh, even though it was too sensitive to the external loads.

Considering these results acquired during the characterization process, we also determined that the repeatability of these actuators is very high since the conductive knits are highly stable with regard to repetitive actuation. For comparison, considering the actuator proposed in [11] in which the conductive liquid was used in microchannels for sensing actuator contractions, it lacks repeatability because such actuators can be easily punctured between the microchannels, which might result in leakage. Thus, since continuous strain variation in the sensing system may result in sensor behavior changing frequently, we tested the proposed actuator several thousands

of the repetitive actuation. Our actuators did not show any physical degradation, indicating their very high performance in terms of actuation life. In other research using a conductive mesh [16], the sensor was found to be heavily vulnerable in environments where other mechanical instruments are used with magnetic fields; however, this effect can be alleviated by using high resistance covers. Additionally, the filters already suggested in this paper that make noises should be removed when measuring actuator contractions. Conductive fibers used with these actuators [15], were shown to be only slightly effective, but the results presented in the related study were somewhat unstable due to the presence of noise. Also note that noise can degrade the performance in the long term, potentially even breaking down, as the actuator tension is directly transferred to these conductive fibers producing friction over these fibers. However, in our approach, we utilized the conductive part of the actuator strictly for sensing, apart from the production of tension for actuation. As a result, even if loads are added, the proposed actuators will not heavily impact the lifetime of the sensing mechanism for the actuator.

The hysteresis effect of the type *B* k-PAM actuator was small, but that of type *C* was very apparent. Recent computing power increases and neural network algorithms will be helpful for overcoming the hysteresis effect, which remains an important issue. Finally, the closed-loop control strategy for k-PAM actuators was suggested to validate their use as standalone actuators without the need of external sensors. In detail, the gain scheduled PID controller was designed to improve the set-point regulation control performance. In addition, a more detailed study on the hysteresis behavior and long-term use of the proposed k-PAM actuators will appear in future research.

REFERENCES

[1] R. H. Gaylord, "Fluid actuated motor system and stroking device," U.S. Patent 2 238 058, Apr. 15, 1941.
[2] H. F. Schulte, D. F. Adamski, and J. R. Pearson. (1961). *Characteristics Braided Fluid Actuator*. [Online]. Available: https://deepblue.lib.umich.edu/handle/2027.42/7479/
[3] M. Ding, J. Ueda, and T. Ogasawara, "Pinpointed muscle force control using a power-assisting device: System configuration and experiment," in *Proc. 2nd IEEE RAS EMBS Int. Conf. Biomed. Robot. Biomechatron.*, Oct. 2000, pp. 181–186.
[4] Y.-L. Park, J. Santos, K. G. Galloway, E. C. Goldfield, and R. J. Wood, "A soft wearable robotic device for active knee motions using flat pneumatic artificial muscles," in *Proc. IEEE Int. Conf. Robot. Automat. (ICRA)*, Jun. 2014, pp. 4805–4810.
[5] R. Bogue, "Exoskeletons and robotic prosthetics: A review of recent developments," *Ind. Robot, Int. J.*, vol. 36, no. 5, pp. 421–427, 2009.
[6] M. Wehner, B. Quinlivan, P. M. Aubin, E. Martinez-Villalpando, M. Baumann, L. Stirling, K. Holt, R. Wood, and C. Walsh, "A lightweight soft exosuit for gait assistance," in *Proc. IEEE Int. Conf. Robot. Automat.*, May 2013, pp. 3362–3369.
[7] C.-P. Chou and B. Hannaford, "Measurement and modeling of McKibben pneumatic artificial muscles," *IEEE Trans. Robot. Autom.*, vol. 12, no. 1, pp. 90–102, Feb. 1996.
[8] M. Doumit, A. Fahim, and M. Munro, "Analytical modeling and experimental validation of the braided pneumatic muscle," *IEEE Trans. Robot.*, vol. 25, no. 6, pp. 1282–1291, Dec. 2009.
[9] S. Davis, N. Tsagarakis, J. Canderle, and D. Caldwell, "Enhanced modeling and performance in braided pneumatic muscle actuators," *Int. J. Robot. Res.*, vol. 22, no. 3, pp. 213–227, Mar. 2003.
[10] B. Tondu and P. Lopez, "Modeling and control of McKibben artificial muscle robot actuators," *IEEE Control Syst. Mag.*, vol. 20, no. 2, pp. 15–38, Apr. 2000.
[11] Y.-L. Park and R. J. Wood, "Smart pneumatic artificial muscle actuator with embedded microfluidic sensing," in *Proc. IEEE SENSORS*, Nov. 2013, pp. 1–4.
[12] L. O. Tiziani, T. W. Cahoon, and F. L. Hammond, "Sensorized pneumatic muscle for force and stiffness control," in *Proc. IEEE Int. Conf. Robot. Automat. (ICRA)*, Jun. 2017, pp. 5545–5552.
[13] J. P. King, L. E. Valle, N. Pol, and Y.-L. Park, "Design, modeling, and control of pneumatic artificial muscles with integrated soft sensing," in *Proc. IEEE Int. Conf. Robot. Automat. (ICRA)*, Jun. 2017, pp. 4985–4990.
[14] S. Kuriyama, M. Ding, Y. Kurita, T. Ogasawara, and J. Ueda, "Flexible sensor for Mckibben pneumatic actuator," in *Proc. IEEE SENSORS*, Oct. 2009, pp. 520–525.
[15] J. Misumi, S. Wakimoto, and K. Suzumori, "Experimental investigation of conductive fibers for a smart pneumatic artificial muscle," in *Proc. IEEE Int. Conf. Robot. Biomimetics (ROBIO)*, Dec. 2015, pp. 2335–2340.
[16] W. Felt, K. Y. Chin, and C. D. Remy, "Contraction sensing with smart braid McKibben muscles," *IEEE/ASME Trans. Mechatronics*, vol. 21, no. 3, pp. 1201–1209, Jun. 2016.
[17] G. Andrikopoulos, G. Nikolakopoulos, S. Manesis, "Advanced nonlinear PID-based antagonistic control for pneumatic muscle actuators," *IEEE Trans. Ind. Electron.*, vol. 61, no. 12, pp. 6926–6937, Dec. 2014.
[18] G. Andrikopoulos, G. Nikolakopoulos, I. Arvanitakis, and S. Manesis, "Piecewise affine modeling and constrained optimal control for a pneumatic artificial muscle," *IEEE Trans. Ind. Electron.*, vol. 61, no. 2, pp. 904–916, Feb. 2014.
[19] D. Zhang, X. Zhao, and J. Han, "Active model-based control for pneumatic artificial muscle," *IEEE Trans. Ind. Electron.*, vol. 64, no. 2, pp. 1686–1695, Feb. 2017.
[20] R. Paradiso, G. Loriga, and N. Taccini, "A wearable health care system based on knitted integrated sensors," *IEEE Trans. Inf. Technol. Biomed.*, vol. 9, no. 3, pp. 337–344, Sep. 2005.
[21] T. Yoshikai, H. Fukushima, M. Hayashi, and M. Inaba, "Development of soft stretchable knit sensor for humanoids' whole-body tactile sensibility," in *Proc. 9th IEEE-RAS Int. Conf. Humanoid Robots*, Dec. 2009, pp. 624–631.
[22] S. Majumder, T. Mondal, and M. J. Deen, "Wearable sensors for remote health monitoring," *Sensors*, vol. 17, no. 1, p. 130, Jan. 2017.
[23] B. Jamil, S. Lee, and Y. Choi, "Conductive knit-covered pneumatic artificial muscle (k-PAM) actuator," in *Proc. IEEE/RSJ Int. Conf. Intell. Robots Syst. (IROS)*, Oct. 2018, pp. 1476–1481.
[24] X. Huo, L. Ma, X. Zhao, and G. Zong, "Observer-based fuzzy adaptive stabilization of uncertain switched stochastic nonlinear systems with input quantization," *J. Franklin Inst.*, vol. 356, no. 4, pp. 1789–1809, 2019.
[25] H. Wang, P. X. Liu, S. Li, and D. Wang, "Adaptive neural output-feedback control for a class of nonlower triangular nonlinear systems with unmodeled dynamics," *IEEE Trans. Neural Netw. Learn. Syst.*, vol. 29, no. 8, pp. 3658–3668, Aug. 2018.
[26] Y. Tan, M. Xiong, B. Niu, J. Liu, and S. Fei, "Distributed hybrid-triggered H_∞ filter design for sensor networked systems with output saturations" *Neurocomputing*, vol. 315, pp. 261–271, Nov. 2018.

BABAR JAMIL received the bachelor's degree in electronics engineering from the COMSATS Institute of Information and Technology, Pakistan. He is currently pursuing the integrated master's Ph.D. degree with the Department of Electrical and Electronic Engineering, Hanyang University, Ansan, South Korea. His research interests include soft robotics, biorobotics, machine learning, and control and system identification.

SEULAH LEE received the M.S. and Ph.D. degrees in clothing and textiles from Hanyang University, Seoul, South Korea, in 2013 and 2017, respectively. She is currently a Postdoctoral Fellow with the Research Institute of Engineering and Technology, Hanyang University. Her current research interests include wearable sensors, smart textiles, electrodes, and smart clothing design.

YOUNGJIN CHOI (S'01–M'03–SM'11) was born in Seoul, South Korea, in 1970. He received the B.S. degree in precision mechanical engineering from Hanyang University, Seoul, South Korea, in 1994, and the M.S. and Ph.D. degrees in mechanical engineering from POSTECH, Pohang, South Korea, in 1996 and 2002, respectively. Since 2005, he has been a Professor with the Department of Electrical and Electronic Engineering, Hanyang University, Ansan, South Korea. From 2002 to 2005, he was a Senior Research Scientist with the Intelligent Robotics Research Center, Korea Institute of Science and Technology (KIST). From 2011 to 2012, he was a Visiting Researcher with the University of Central Florida, USA. His research interests include biorobotics and control theory. From 2010 to 2014, he was an Associate Editor of the IEEE TRANSACTIONS ON ROBOTICS. From 2016 to 2018, he was an Associate Editor of the IEEE ROBOTICS AND AUTOMATION LETTERS. Since 2018, he has been a Senior Editor of the IEEE ROBOTICS AND AUTOMATION LETTERS.